Dalton Transactions

Cite this: *Dalton Trans.*, 2011, **40**, 1707

www.rsc.org/dalton

PAPER

Nucleophilic reactivity of a series of peroxomanganese(III) complexes supported by tetradentate aminopyridyl ligands†

Robert A. Geiger, Swarup Chattopadhyay, Victor W. Day and Timothy A. Jackson*

Received 11th November 2010, Accepted 3rd December 2010
DOI: 10.1039/c0dt01570a

Peroxomanganese(III) adducts have been postulated as important intermediates in manganese-containing enzymes and small molecule oxidation catalysts. Synthetic peroxomanganese(III) complexes are known to be nucleophilic and facilitate aldehyde deformylation, offering a convenient way to compare relative reactivities of complexes supported by different ligands. In this work, tetradentate dipyridyldiazacycloalkane ligands with systematically perturbed steric and electronic properties were used to generate a series of manganese(II) and peroxomanganese(III) complexes. X-Ray crystal structures of five manganese(II) complexes all show the ligands bound to give *trans* complexes. Treatment of these Mn^{II} precursors with H_2O_2 and Et_3N in MeCN at –40 °C results in the formation of peroxomanganese(III) complexes that differ only in the identity of the pyridine ring substituent and/or the number of carbons in the diazacycloalkane backbone. To determine the effects of small ligand perturbations on the reactivity of the peroxo group, the more thermally stable peroxomanganese(III) complexes were reacted with cyclohexanecarboxaldehyde. For these complexes, the rate of deformylation does not correlate with the expected nucleophilicity of the peroxomanganese(III) unit, as the inclusion of methyl substituents on the pyridines affords slower deformylation rates. It is proposed that adding methyl-substituents to the pyridines, or increasing the number of carbons on the diazacycloalkane, sterically hinders nucleophilic attack of the peroxo ligand on the carbonyl carbon of the aldehyde.

Introduction

Peroxoiron(III) and peroxomanganese(III) complexes play important roles in biological systems and in catalytic oxidation reactions. A ferric-peroxo species is implicated as a key intermediate in certain cytochrome P450-catalyzed reactions, including the aromatization of androgen to estrogen by cytochrome P450 aromatase[1] and oxidation of L-arginine to citrulline by the P450 monooxygenase nitric oxide synthase.[2] Peroxomanganese(III) complexes are potential intermediates in manganese containing enzymes, including manganese superoxide dismutase, manganese catalase, and manganese ribonucleotide reductase.[3–7] While the mechanisms of these systems remain the subject of much current work, the importance of peroxo-level intermediates has been outlined in several reports.[8–11] An example is the manganese superoxide dismutase enzyme that forms a product-inhibited complex proposed to contain a peroxomanganese(III) adduct.[8,9,12]

A variety of different ligands sets, ranging from neutral, tetraamine macrocylic ligands to anionic, facially-coordinating tris(pyrazolyl)borate chelates, have been use to stabilize peroxomanganese(III) intermediates.[13–21] Of the structurally characterized complexes, all exhibit side-on (η^2) peroxo ligands with Mn–O distances in the range of 1.85 to 1.88 Å,[13,15,16,21,22] although it has been proposed that this distance can be modulated by the inclusion of electron-donating groups *trans*[16] or *cis*[20] to the peroxo unit. A convenient way to compare the relative reactivities of these diverse complexes, and thus define different steric and electronic influences on reactivity, is by using a common reaction. Because aldehyde deformylation appears to be characteristic of both Mn^{III}-peroxo[15,16] and Fe^{III}-peroxo[23,24] complexes, it is ideal for this purpose. Indeed, peroxomanganese(III) adducts assembled using very different supporting ligands (Scheme 1) deformylate cyclohexanecarboxaldehyde (CCA).[15–17] For Mn^{III}–O_2 adducts supported by the 14-TMC and 13-TMC ligands (14-TMC = 1,4,8,11-tetramethyl-1,4,8,11-tetraazacyclotetradecane and 13-TMC = 1,4,7,10-tetramethyl-1,4,7,10-tetraazacyclotridecane), nearly identical second-order rate constants were reported (k_2 = 2.4 and 1.2 M^{-1} min^{-1} respectively at 10 °C). Cyclohexene, the expected product of CCA deformylation (Scheme 1), was observed in both cases in ~55% yield.[15,16] Using a peroxomanganese(III) complex supported by the anionic H_3bupa ligand (H_3bupa is the dianion of bis[(*N′-tert*-butylurealey)-*N*-ethyl]-(6-pivalamido-2-pyridylmethyl)amine), Borovik *et al.* reported the oxidative deformylation of CCA to give cyclohexanone in 40% yield.[17]

Department of Chemistry, University of Kansas, 1251 Wescoe Hall Drive, Lawrence, KS 66045, USA. E-mail: taj@ku.edu; Fax: +1 (785) 864-5396; Tel: +1 (785) 864-3968

† Electronic supplementary information (ESI) available. CCDC reference numbers 801091–801095. For ESI and crystallographic data in CIF or other electronic format see DOI: 10.1039/c0dt01570a

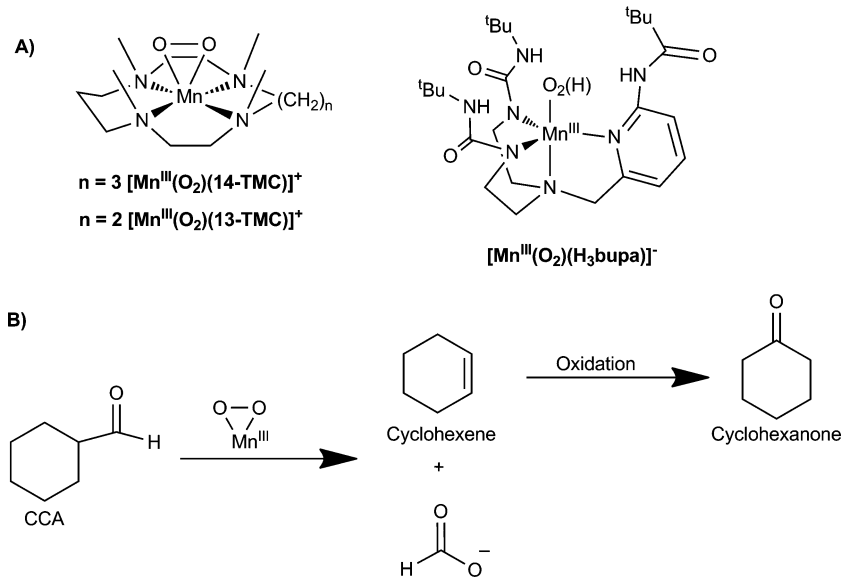

Scheme 1

The identity of the ligand *trans* to the peroxo group has been shown to have a dramatic effect on the rate of CCA deformylation. The addition of anions to $[Mn^{III}(O_2)(13\text{-TMC})]^+$ leads to the formation of neutral, seven-coordinate Mn^{III}–O_2 adducts, formulated as $[Mn^{III}(O_2)(13\text{-TMC})(X)]$ (where $X^- = CN^-$, NCS^-, $CF_3CO_2^-$, and N_3^-) that showed dramatically enhanced rates for CCA deformylation.[16] In particular $[Mn^{III}(O_2)(13\text{-TMC})(N_3)]$ displayed a second-order rate constant 10^4 larger than that of $[Mn^{III}(O_2)(13\text{-TMC})]^+$. This remarkably large rate enhancement was attributed to the strong electron donating properties of the axial azide ligand. It was postulated that the *trans* N_3^- ligand favors a peroxo binding mode intermediate between side-on and end-on, increasing the nucleophilicity of one oxygen atom of the peroxo ligand.

We have recently reported a series of Mn^{III}–O_2 complexes supported by tetradentate dipyridyldiazacycloalkane ligands: $L^7py_2^H$, $L^7py_2^{5\text{-Br}}$, $L^7py_2^{6\text{-Me}}$, and $L^7py_2^{6\text{-MeO}}$ ($L^7py_2^H$ = 1,4-bis(2-pyridylmethyl)-1,4-diazepane; see Scheme 2).[20] It was shown that by changing the substituent on the pyridine ring, the spectroscopic properties and stability of these peroxomanganese(III) complexes were perturbed. For $[Mn^{III}(O_2)(L^7py_2^H)]^+$ and $[Mn^{III}(O_2)(L^7py_2^{6\text{-Me}})]^+$, these spectroscopic changes were linked to the geometric and electronic structure of the Mn^{III}–O_2 unit. Specifically we proposed that the inclusion of the electron-donating methyl-substituents lead to an elongation in one of the Mn–O bonds, affording a more asymmetric, end-on binding mode. In accordance with the reactivity studies described above, this should render the peroxo in $[Mn^{III}(O_2)(L^7py_2^{6\text{-Me}})]^+$ more nucleophilic than that of $[Mn^{III}(O_2)(L^7py_2^H)]^+$. To evaluate this prediction and further explore steric and electronic influences on reactivity, in this current work we performed systematic ligand modifications by altering (i) the nature and location of pyridine ring substituents, (ii) the size of the diazacycloalkane backbone, and (iii) the type of N-ligand from pyridine to quinoline (Scheme 2). The structures of the manganese(II) precursors were solved by X-ray diffraction, and their geometries report the effects of these ligand perturbations. In cases where these new ligands supported stable peroxomanganese(III) adducts, these species were reacted with CCA to determine the effect of ligand modifications on the rate of CCA deformylation. Unlike previous observations, CCA deformylation by the Mn^{III}–O_2 units in these complexes appears to be largely influence by the sterics of the supporting ligand.

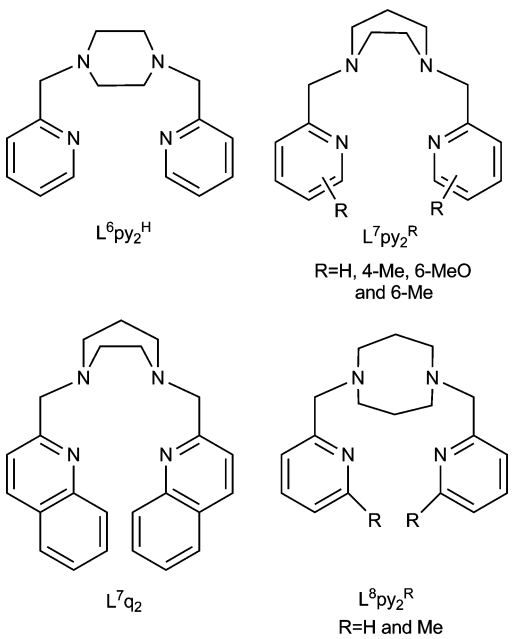

Scheme 2

Results and discussion

To complement our previously reported peroxomanganese(III) complexes generated using the $L^7py_2^H$, $L^7py_2^{6\text{-Me}}$, and $L^7py_2^{6\text{-MeO}}$ ligands,[20] we assembled five new Mn^{II} complexes using the $L^6py_2^H$, $L^7py_2^{4\text{-Me}}$, L^7q_2, $L^8py_2^H$, and $L^8py_2^{6\text{-Me}}$ ligands (Scheme 2). With these new ligands, our initial objective was to assess the effects of four variables on the stability and reactivity of the Mn^{III}–O_2 unit.

Table 1 Selected bond lengths (Å) and angles (°) for manganese(II) complexes

Complex	Mn–N(1)	Mn–N(2)	Mn–N(3)	Mn–N(4)	Mn–X(1)	Mn–X(2)	Mn–X(3)[a]	N3–Mn–N4	C1–N1–Mn–N2–C11
$[Mn^{II}(L^{6}py_2^{H})(NCMe)_3](ClO_4)_2$	2.313(2)	2.307(2)	2.339(2)	2.360(3)	2.286(3)[a]	2.314(2)[a]	2.370(3)	62.82(8)	−57.0(3)
$[Mn^{II}(L^{7}py_2^{H})(NCMe)_3](ClO_4)_2$[b]	2.306(9)	2.308(3)	2.369(3)	2.357(3)	2.268(2)[a]	2.311(2)[a]	2.478(2)	67.40(1)	−66.3(6)
$[Mn^{II}(L^{7}py_2^{6\text{-}Me})(ClO_4)_2]$[b]	2.283(2)	2.284(2)	2.30692)	2.285(2)	2.212(2)[c]	2.280(2)[a]	NA	69.50(7)	−48.1(2)
$[Mn^{II}(L^{7}py_2^{4\text{-}Me})(OTf)_2]$	2.216(2)	2.213(2)	2.288(2)	2.277(2)	2.198(2)[d]	2.235(2)[d]	NA	71.13(6)	−44.5(2)
$[Mn^{II}(L^{7}py_2^{6\text{-}MeO})(ClO_4)_2]$[b]	2.176(2)	2.176(2)	2.308(2)	2.308(2)	2.278(2)[c]	2.278(2)[c]	NA	70.36(9)	−43.2(2)
$[Mn^{II}(L^{7}q_2)(ClO_4)_2]$	2.226(2)	2.254(2)	2.274(2)	2.263(2)	2.209(1)[c]	2.282(1)[c]	NA	70.77(6)	−42.1(2)
$[Mn^{II}(L^{8}py_2^{H})(ClO_4)_2]$	2.246(1)	2.257(1)	2.292(1)	2.320(1)	2.244(1)[c]	2.266(1)[c]	NA	78.08(5)	−68.7(1)
$[Mn^{II}(L^{8}py_2^{6\text{-}Me})(OTf)_2]$	2.273(1)	2.273(1)	2.290(1)	2.290(1)	2.205(1)[d]	2.205(1)[d]	NA	76.27(4)	−62.2(1)

[a] X = N(CMe). [b] From reference 20. [c] X = $O(ClO_3)^-$. [d] X = OTf.

These variables are (i) nature of the pyridine substituent ($L^{7}py_2^{H}$ *versus* $L^{7}py_2^{6\text{-}Me}$ and $L^{8}py_2^{H}$ *versus* $L^{8}py_2^{6\text{-}Me}$), (ii) position of the pyridine substituent ($L^{7}py_2^{6\text{-}Me}$ *versus* $L^{7}py_2^{4\text{-}Me}$), (iii) size of the diazacycloalkane backbone ($L^{6}py_2$ *versus* $L^{7}py_2$ and $L^{8}py_2$), and (iv) identity of the N-donor ligand ($L^{7}py_2$ *versus* $L^{7}q_2$).

Structural properties of manganese(II) complexes

Fig. 1 displays ORTEP diagrams for the five manganese(II) complexes $[Mn^{II}(L^{6}py_2^{H})(NCMe)_3](ClO_4)_2$, $[Mn^{II}(L^{7}py_2^{4\text{-}Me})(OTf)_2]$, $[Mn^{II}(L^{7}q_2)(ClO_4)_2]$, $[Mn^{II}(L^{8}py_2^{H})(ClO_4)_2]$, and $[Mn^{II}(L^{8}py_2^{6\text{-}Me})(OTf)_2]$. Selected bond distances are given in Table 1. For each of the five complexes, the linear, tetradentate ligand is bound in the *trans* conformation, creating two axial coordination sites occupied by solvent ($L^{6}py_2^{H}$) or anionic ligands (ClO_4^- for $L^{7}q_2$ and $L^{8}py_2^{H}$, and OTf^- for $L^{7}py_2^{4\text{-}Me}$ and $L^{8}py_2^{6\text{-}Me}$). In the case of $[Mn^{II}(L^{6}py_2^{H})(NCMe)_3](ClO_4)_2$, a seventh ligand is bound in the equatorial plane, giving a near pentagonal bipyramidal geometry around the Mn(II) center. For all the complexes, the Mn^{II}–ligand bond lengths range from ~2.1 to 2.5 Å, indicative of high-spin manganese(II) centers.

The differences in geometry of the Mn(II) complexes supported by the $L^{6}py_2^{H}$, $L^{7}py_2^{H}$, and $L^{8}py_2^{H}$ ligands are directly related to the variation in diazacycloalkane ring size. The $[Mn^{II}(L^{8}py_2^{H})(ClO_4)_2]$ complex is six-coordinate, while the corresponding $L^{7}py_2^{H}$ and $L^{6}py_2^{H}$ complexes display seven-coordinate Mn(II) centers. Although heptacoordinate Mn(II) complexes are not unusual,[25–28] they are far less common than six-coordinate analogues. We attribute the structural differences among these ligands to the variation in N3–Mn–N4 bite angle as a function of the diazacycloalkane ring size (although the identity of the X ligand, NCMe or ClO_4^-, will also be important). When bound to the Mn^{II} center, the $L^{6}py_2^{H}$ ligand creates a N3–Mn–N4 bite angle of 62.8°, which is smaller than those of the corresponding $L^{7}py_2^{H}$ and $L^{8}py_2^{H}$ complexes (67.4° and 78.1°, respectively). Equatorial angles of 72° are expected for idealized pentagonal bipyramidal complexes, consistent with $[Mn^{II}(L^{6}py_2^{H})(NCMe)_3]^{2+}$ and $[Mn^{II}(L^{7}py_2^{H})(NCMe)_3]^{2+}$ being seven-coordinate. The bite angles also offer a rationale for the smaller meridional Mn–NCMe bond length for $[Mn^{II}(L^{6}py_2^{H})(NCMe)_3]^{2+}$ compared with $[Mn^{II}(L^{7}py_2^{H})(NCMe)_3]^{2+}$ (2.37 *versus* 2.48 Å, respectively; see Mn–X_3 in Table 1). Binding of a fifth equatorial ligand is also associated with significant canting of the pyridines, as assessed by the torsional angle resulting from the two planes of the pyridine rings (Table 1). This canting is nicely illustrated pictorially in the space-filling model of $[Mn^{III}(L^{6}py_2^{H})]^{2+}$ shown in Fig. 1F.

In all cases, the inclusion of pyridine substituents, or substitution of pyridines for quinolines, results in six-coordinate complexes. On the basis of their small N3–Mn–N4 bite angles of ~70° (Table 1), the Mn^{II} complexes supported by the $L^{7}q_2$ ligand and the substituted $L^{7}py_2^{R}$ ligands (R = 6-Me, 6-MeO, and 4-Me) should be able to accommodate a fifth equatorial ligand. For the $L^{7}py_2^{6\text{-}Me}$, $L^{7}py_2^{6\text{-}MeO}$, and $L^{7}q_2$ complexes, steric crowding of the equatorial plane hinders the binding of a seventh ligand. For the $[Mn^{II}(L^{7}py_2^{4\text{-}Me})(OTf)_2]$ complex, the lack of heptacoordination is tentatively attributed to the shorter Mn–N(pyridine) bonds relative to $[Mn^{II}(L^{7}py_2^{H})(NCMe)_3]^{2+}$ (2.22 *versus* 2.31 Å, respectively; Table 1), which are due to the electron-donating 4-Me groups. These shorter distances for $[Mn^{II}(L^{7}py_2^{4\text{-}Me})(OTf)_2]$ further crowd the equatorial plane and lead to similar pyridine ring canting when compared with the $L^{7}py_2^{6\text{-}Me}$ and $L^{7}py_2^{6\text{-}MeO}$ analogues that must cant to avoid steric clashing between the 6-substituents. Alternatively, the lower coordination number of $[Mn^{II}(L^{7}py_2^{4\text{-}Me})(OTf)_2]$ could be attributed to crystallization of the triflate-coordinated complex, as opposed to the solvent-coordinated analogue, which would arise from the relative solubilities of these two forms under the crystallization conditions. The bulk of the triflate ligands would then disfavor heptacoordination. Space-filling models highlighting the general steric effects observed in the crystal structures are including in Supplementary Information (Fig. S1, ESI†).

Formation of peroxomanganese(III) complexes

The absorption spectra of acetonitrile solutions of the five new manganese(II) complexes, $[Mn^{II}(L^{6}py_2^{H})(NCMe)_3]^{2+}$, $[Mn^{II}(L^{7}py_2^{4\text{-}Me})(OTf)_2]$, $[Mn^{II}(L^{7}q_2)(ClO_4)_2]$, $[Mn^{II}(L^{8}py_2^{H})(ClO_4)_2]$, and $[Mn^{II}(L^{8}py_2^{6\text{-}Me})(OTf)_2]$, are featureless at energies below 33 000 cm^{-1}, indicative of high spin manganese(II) centers. Treatment of the $[Mn^{II}(L^{7}py_2^{4\text{-}Me})]^{2+}$, $[Mn^{II}(L^{7}q_2)]^{2+}$, and $[Mn^{II}(L^{8}py_2^{H})]^{2+}$ complexes with 5 equivalents H_2O_2 and 0.5 equivalents triethylamine at –40 °C results in the formation of new absorption features in the visible region (Fig. 2 and Table 2). Mass spectrometry experiments on these colored solutions reveal major ion peaks consistent with $[Mn^{III}(O_2)(L^{7}py_2^{4\text{-}Me})]^+$, $[Mn^{III}(O_2)(L^{7}q_2)]^+$, and $[Mn^{III}(O_2)(L^{8}py_2^{H})]^+$. Thus, these Mn^{II} centers form metastable Mn^{III}–O_2 adducts when reacted with H_2O_2 in the presence of base at low temperature (Scheme 3), consistent with a previous report on similar complexes.[20] While $[Mn^{II}(L^{8}py_2^{6\text{-}Me})]^{2+}$ reacts with 5 equivalents H_2O_2 and 0.5 equivalents triethylamine at –40 °C to form a colored intermediate, the fleeting nature of this chromophore ($t_{1/2}$ = seconds at –40 °C) prevented its further characterization.

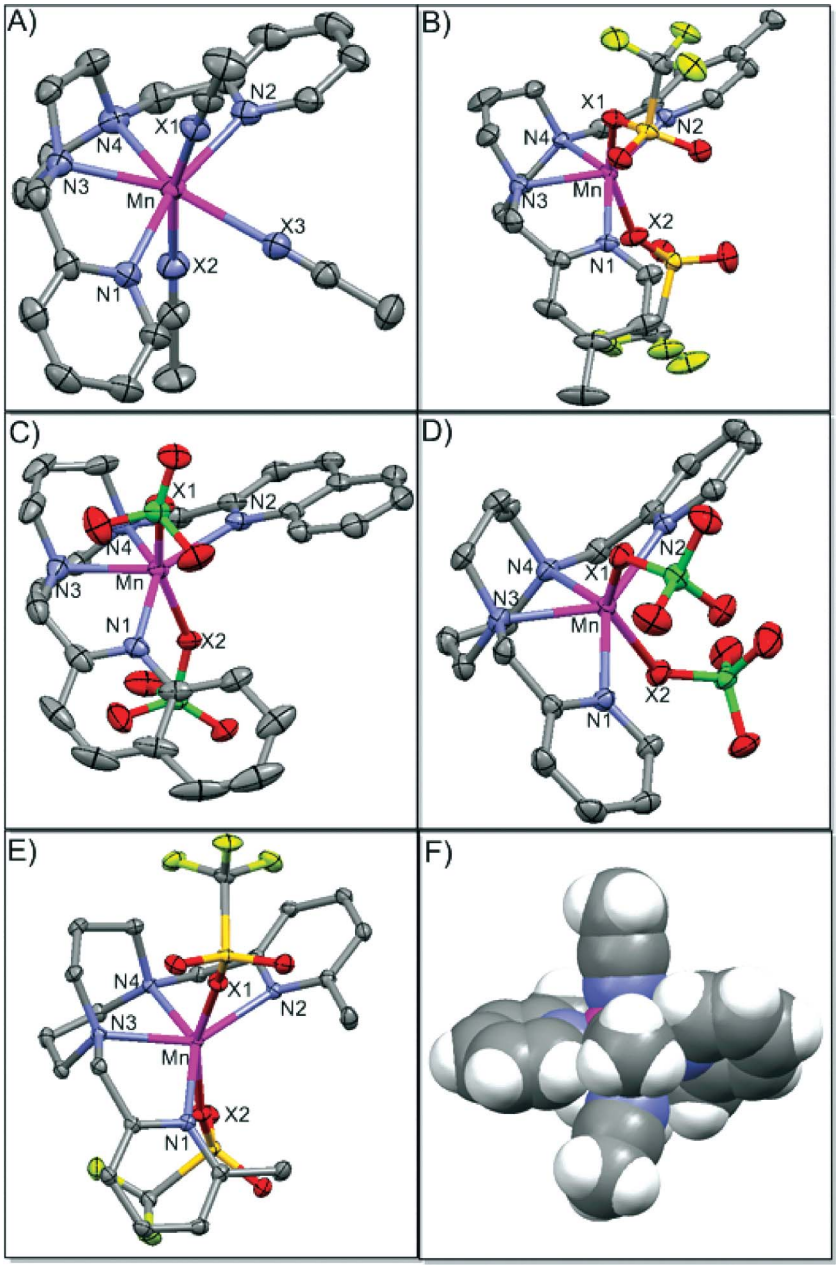

Fig. 1 ORTEP diagrams of (A) $[Mn^{II}(L^{6}py_{2}^{H})(NCMe)_{3}](ClO_{4})_{2}$, (B) $[Mn^{II}(L^{7}py_{2}^{4\text{-}Me})(OTf)_{2}]$, (C) $[Mn^{II}(L^{7}q_{2})(ClO_{4})_{2}]$, (D) $[Mn^{II}(L^{8}py_{2}^{H})(ClO_{4})_{2}]$, and (E) $[Mn^{II}(L^{8}py_{2}^{6\text{-}Me})(OTf)_{2}]$ showing 50% probability thermal ellipsoids. (F) Space filling model for $[Mn^{II}(L^{6}py_{2}^{H})(NCMe)_{3}]^{2+}$ viewed along the Mn–X_3 axis. For ORTEP structures, hydrogen atoms and noncoordinating counteranions have been removed for clarity. Significant interatomic distances and angles are listed in Table 1.

Notably, $[Mn^{II}(L^{6}py_{2}^{H})]^{2+}$ showed no reaction under these conditions.

The absorption maxima of $[Mn^{III}(O_2)(L^{7}py_{2}^{4\text{-}Me})]^{+}$ and $[Mn^{III}(O_2)(L^{8}py_{2}^{H})]^{+}$ are nearly identical to those of $[Mn^{III}(O_2)(L^{7}py_{2}^{H})]^{+}$, consisting of a weak feature at ~17 000 cm^{-1} and a more intense band at ~22 000 cm^{-1} (Table 2). In contrast, the absorption spectrum of $[Mn^{III}(O_2)(L^{7}q_{2})]^{+}$ resembles that of $[Mn^{III}(O_2)(L^{7}py_{2}^{6\text{-}Mc})]^{+}$ and $[Mn^{III}(O_2)(L^{7}py_{2}^{6\text{-}MeO})]^{+}$ ($\lambda_{max} \approx 16\,000$ and 24 000 cm^{-1}). Among this set of complexes, the common link between ligand structure and absorption maxima is steric bulk in the 6-position of the pyridine ring (assuming the quinoline as a "bulky" pyridine). With the aid of density functional theory (DFT) computations, we previously attributed differences in absorption and, especially, magnetic circular dichroism (MCD) spectra of $[Mn^{III}(O_2)(L^{7}py_{2}^{H})]^{+}$ and $[Mn^{III}(O_2)(L^{7}py_{2}^{6\text{-}Me})]^{+}$ to a change from a side-on-bound peroxo ligand with identical Mn–O_{peroxo} distances of 1.87 Å in the former complex to a more end-on peroxo with Mn–O_{peroxo} distances of 1.87 and 1.91 Å in the latter species.[20] It was suggested that the increased Lewis acidity of the manganese center in $[Mn^{III}(O_2)(L^{7}py_{2}^{6\text{-}Me})]^{+}$ led to the longer, asymmetric Mn–O_{peroxo} bond lengths. The data presented in Table 2 suggests an alternative explanation. The inclusion of

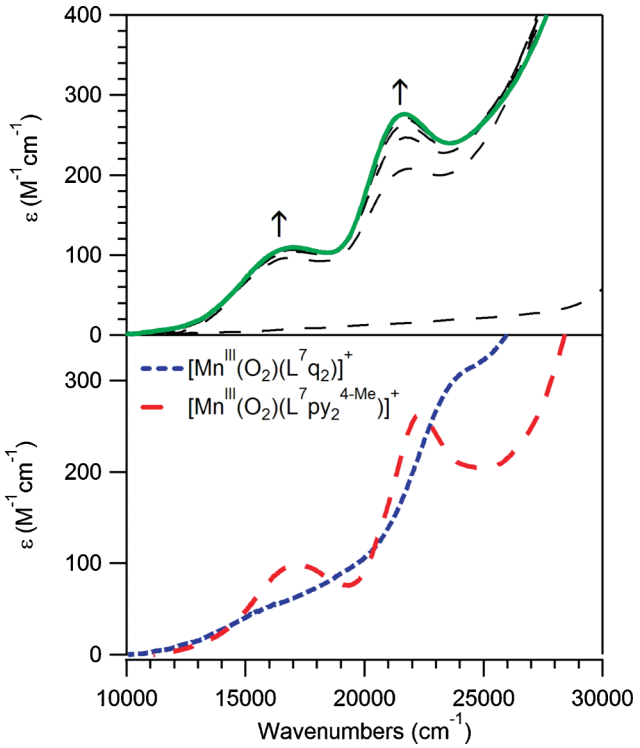

Fig. 2 Top: Formation of $[Mn^{III}(O_2)(L^8py_2{}^H)]^+$ after the addition of 5 equivalents H_2O_2 and 0.5 equivalents triethylamine of at –40 °C in MeCN. Bottom: Electronic absorption spectra of $[Mn^{III}(O_2)(L^7q_2)]^+$ and $[Mn^{III}(O_2)(L^7py_2{}^{4\text{-Me}})]^+$ at –40 °C in MeCN.

bulky groups in the 6-position is expected to cause significant canting of the pyridine rings, as evidenced in the XRD structures of the Mn(II) complexes (Fig. 1 and Table 1). This increased canting causes the 6-substituents to partially block the axial positions, sterically disfavoring the formation of a symmetric, side-on peroxo ligand in the $L^7py_2{}^{6\text{-Me}}$, $L^7py_2{}^{6\text{-MeO}}$, and L^7q_2 complexes. Importantly, this model would also account for the similarities of the absorption maxima of the $[Mn^{III}(O_2)(L^7py_2{}^H)]^+$ and $[Mn^{III}(O_2)(L^7py_2{}^{4\text{-Me}})]^+$ complexes.

Reactivity of peroxomanganese(III) complexes

The addition of excess CCA to the green acetonitrile solution of $[Mn^{III}(O_2)(L^7py_2{}^H)]^+$ at –40 °C, led to the disappearance of the characteristic visible bands at 22 470 and 16 950 cm^{-1}, indicating the decay of the peroxomanganese(III) complex (Fig. 3A). This decay followed pseudo-first order behavior when excess CCA was used. By plotting the range of pseudo-first order rate constants (k_{obs}) as a function of CCA concentration, we determined a second-order-rate constant (k_2) of 3.11 M^{-1} min^{-1} at –40 °C (Fig. 3B). Reactions performed with either perchlorate or triflate as counteranion displayed identical rates. The organic product of this reaction was determined by GC-MS, and cyclohexanone was identified in ~50% yield based on the concentration of the peroxomanganese(III) complex. No other organic products were detected. The formation of a ketone product in aldehyde deformylation has been previously observed for other peroxoiron(III)[23,24] and peroxomanganese(III)[17] complexes.

To date the most reactive peroxomanganese(III) complex for CCA deformylation is $[Mn^{III}(O_2)(13\text{-TMC})(N_3)]$.[16] Using the $\Delta H^{\ddagger}$ and $\Delta S^{\ddagger}$ values reported for this reaction, we estimate a k_2 value of ~220 M^{-1} min^{-1} at –40 °C, which is 10^2-fold larger than that of $[Mn^{III}(O_2)(L^7py_2{}^H)]^+$. On the basis of this comparison, as well as the other reactivity data reported by Nam *et al.* for the series of $[Mn^{III}(O_2)(13\text{-TMC})(X)]$ complexes,[16] this implies that the k_2 value of $[Mn^{III}(O_2)(L^7py_2{}^H)]^+$ is comparable to that of $[Mn^{III}(O_2)(13\text{-TMC})(CN)]$ and 10^2-fold greater than that of the parent complex, $[Mn^{III}(O_2)(13\text{-TMC})]^+$. Thus, $[Mn^{III}(O_2)(L^7py_2{}^H)]^+$ represents the fastest Mn^{III}–O_2 CCA deformylation agent lacking an anionic ligand.

The nucleophilic nature of the aldehyde deformylation reaction was confirmed by reacting $[Mn^{III}(O_2)(L^7py_2{}^H)]^+$ with

Table 2 Properties of peroxomanganese(III) complexes

Complex	λ_{max}/cm^{-1} (ε/M^{-1} cm^{-1})	$t_{1/2}$ at 0 °C
$[Mn^{III}(O_2)(L^7py_2{}^H)]^+$[a]	22 470 (280) 16 950 (120)	15 min
$[Mn^{III}(O_2)(L^7py_2{}^{6\text{-Me}})]^+$[a]	24 100 (280) ~16 130 (80)	6 min
$[Mn^{III}(O_2)(L^7py_2{}^{6\text{-MeO}})]^+$[a]	24 000 (250) 17 900 (80)	~ seconds
$[Mn^{III}(O_2)(L^7py_2{}^{4\text{-Me}})]^+$	22 470 (260) ~17 000 (100)	6 min
$[Mn^{III}(O_2)(L^7q_2)]^+$	24 050 (305) ~16 500 (70)	4 min
$[Mn^{III}(O_2)(L^8py_2{}^H)]^+$	21 550 (280) 16 700 (120)	12 min

[a] From reference 20.

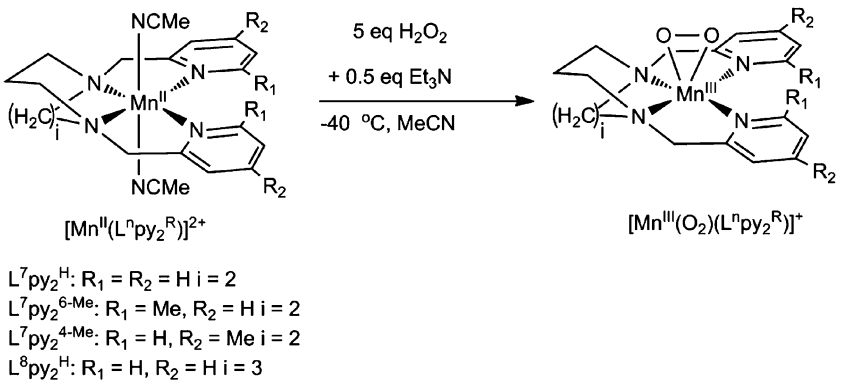

$L^7py_2{}^H$: $R_1 = R_2 = H$ i = 2
$L^7py_2{}^{6\text{-Me}}$: R_1 = Me, R_2 = H i = 2
$L^7py_2{}^{4\text{-Me}}$: R_1 = H, R_2 = Me i = 2
$L^8py_2{}^H$: $R_1 = R_2 = H$ i = 3

Scheme 3

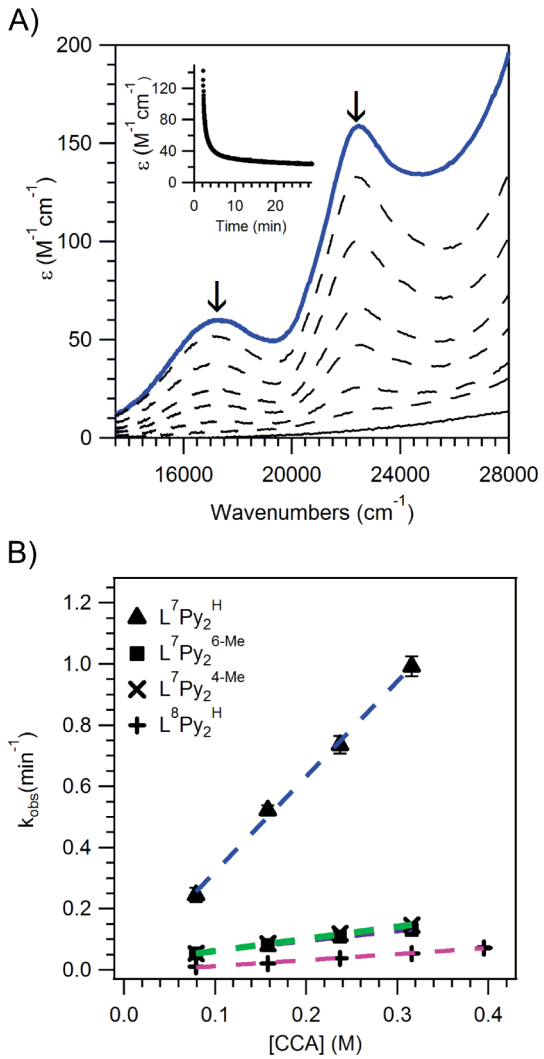

Fig. 3 (A) Electronic absorption spectral changes for $[Mn^{III}(O_2)(L^7py_2{}^H)]^+$ (2.5 mM) upon addition of cyclohexanecarboxaldehyde (60 equivalents, 150 mM) at –40 °C in MeCN. Insert shows the time course of the absorbance at 23 000 cm^{-1}. (B) k_{obs} *versus* cyclohexanecarboxaldehyde concentration. Error bars represent two standard deviations determined from 3 or 4 replicate experiments.

para-substituted benzaldehydes (Cl, H, Me, and OMe). Because the deformylation reaction presumably involves nucleophilic attack of the peroxo on the carbonyl carbon on the aldehyde, electron withdrawing groups on the substrate should make the reaction more facile. The k_{obs} values for all four *para*-substituted benzaldehydes were determined under invariant conditions of temperature and concentration. The *para*-substituents were found to affect k_{obs} in the manner expected for a nucleophilic reaction (*i.e.*, k_{obs} increased with increasing electron-withdrawing properties: Cl > H > Me > OMe). Indeed, the plot of log k_{obs} *versus* Hammett constants (σ_p) are linear with a ρ value of 1.25, as shown in Fig. 4. Similar values for ρ have been observed for other nucleophilic aldehyde deformylation reactions.[16]

The other three Mn^{III}–O_2 complexes $[Mn^{III}(O_2)(L^7py_2{}^{6\text{-}Me})]^+$, $[Mn^{III}(O_2)(L^7py_2{}^{4\text{-}Me})]^+$, and $[Mn^{III}(O_2)(L^8py_2{}^H)]^+$ were reacted with CCA in a similar manner, and in each case cyclohexanone was observed as the organic product. The second-order-rate

Table 3 Second-order-rate constants for CCA deformylation at –40° C

Complex	k_2/$M^{-1}min^{-1}$
$[Mn^{III}(O_2)(L^7py_2{}^H)]^+$	3.1
$[Mn^{III}(O_2)(L^7py_2{}^{6\text{-}Me})]^+$	0.32
$[Mn^{III}(O_2)(L^7py_2{}^{4\text{-}Me})]^+$	0.40
$[Mn^{III}(O_2)(L^8py_2{}^H)]^+$	0.19

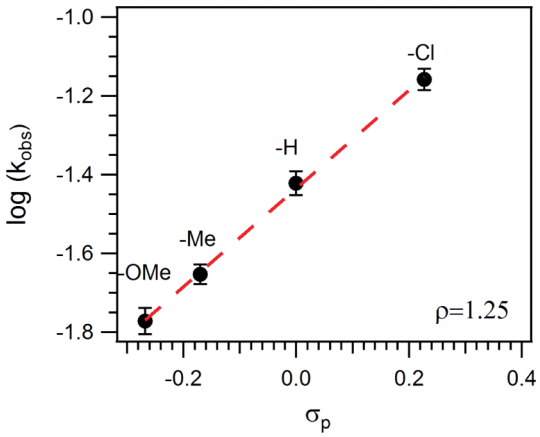

Fig. 4 Hammett correlation of the reaction with *para*-substituted benzaldehydes with $[Mn^{III}(O_2)(L^7py_2{}^H)]^+$. Error bars represent two standard deviations from three replicate experiments.

constants are less than that for $[Mn^{III}(O_2)(L^7py_2{}^H)]^+$ by an order of magnitude (Table 3). Because the rate of aldehyde deformylation is expected to increase as the nucleophilicity of the peroxo ligand increases,[16,23] it is initially surprising that the $[Mn^{III}(O_2)(L^7py_2{}^{6\text{-}Me})]^+$ and $[Mn^{III}(O_2)(L^7py_2{}^{4\text{-}Me})]^+$ complexes, which bear pyridine rings with electron-donating methyl groups, exhibit smaller second-order-rate constants than $[Mn^{III}(O_2)(L^7py_2{}^H)]^+$. We attribute this to steric hindrance of CCA-peroxo interactions caused by canting of the pyridine rings ($L^7py_2{}^{6\text{-}Me}$ and $L^7py_2{}^{4\text{-}Me}$) or the presence of the bulkier 8-membered diazacycloalkane backbone ($L^8py_2{}^H$). In support, Fig. 5 shows space-filling models of $[Mn^{III}(O_2)(L^7py_2{}^H)]^+$, $[Mn^{III}(O_2)(L^7py_2{}^{6\text{-}Me})]^+$ and $[Mn^{III}(O_2)(L^7py_2{}^{4\text{-}Me})]^+$ complexes developed using density functional theory (DFT) geometry optimization. The peroxo ligand in the optimized model of $[Mn^{III}(O_2)(L^7py_2{}^H)]^+$ is the most exposed, whereas the peroxo groups in the other complexes are shielded by the canting of the pyridine rings.

Conclusion

Because peroxomanganese(III) intermediates play an important role in manganese-containing enzymes and small molecule oxidation catalysts, it is important to identify the factors affecting the nucleophilicity of the peroxo ligand. A characteristic reaction of synthetic peroxomanganese(III) complexes is aldehyde deformylation, which offers a convenient method for comparing relative reactivities of peroxomanganese(III) complexes supported by different ligands. Herein, we reported the X-ray structures of a series of manganese(II) complexes with tetradentate dipyridyldiazacycloalkane ligands. Both the size of the diazacycloalkane backbone and the position and identity of the ring substituents have a large influence on the geometry of the Mn(II) complex, with both seven- and six-coordinate complexes observed. Treatment of some

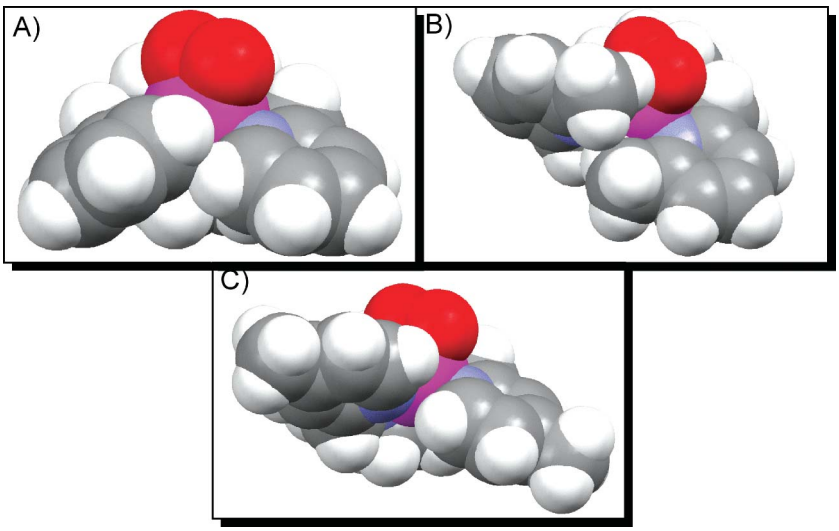

Fig. 5 Space filling models for (A) $[Mn^{III}(O_2)(L^7py_2{}^H)]^+$, (B) $[Mn^{III}(O_2)(L^7py_2{}^{6\text{-}Me})]^+$, and (C) $[Mn^{III}(O_2)(L^7py_2{}^{4\text{-}Me})]^+$ based on structures derived from DFT energy minimizations.

of these manganese(II) complexes with H_2O_2/Et_3N at –40 °C resulted in the formation of peroxomanganese(III) adducts. The thermally stable complexes were treated with CCA to determine the effects of small ligand perturbations on the reactivity of the peroxo group. $[Mn^{III}(O_2)(L^7py_2{}^H)]^+$ was observed to have the largest second-order rate constant (k_2), by an order of magnitude, compared to the other complexes. This result was initially surprising because the electron rich $L^7py_2{}^{4\text{-}Me}$ and $L^7py_2{}^{6\text{-}Me}$ ligands were expected to increase the nucleophilicity of the peroxo. $[Mn^{III}(O_2)(L^8py_2{}^H)]^+$ was observed to have the slowest k_2 value. The decrease in k_2 values was attributed to the steric hindrance of nucleophilic attack of the peroxo ligand on the carbonyl carbon of the aldehyde. This is the first observation of steric hindrance in aldehyde deformylation reaction for a series of Mn^{III}–O_2 complexes.

Experimental

Materials

All chemicals were obtained from commercial vendors at ACS reagent-grade or better and were used without further purification except for CCA. Fractional distillation at 43 °C was preformed under reduced pressure (10 Torr) to remove acid impurities from CCA. All solvents were dried by routine techniques under an inert argon atmoshphere.[29] Unless otherwise stated, manipulations of Mn^{II} complexes were carried out under argon using a glovebox or Schlenk techniques.

Instrumentation

^{1}H NMR spectra were obtained on a Bruker DRX 400 MHz NMR spectrometer. Electronic absorption spectra were recorded on a Cary 50 Bio spectrophotometer (Varian) or an Agilent 8453 spectrometer, each of which is interfaced with a Unisoku cryostat (USP-203-A). ESI-mass spectrometry experiments were performed using an LCT Primers MicroMass electrospray-ionization time-of-flight instrument. Elemental analysis was performed by Columbia Analytical Services, Tucson AZ. The gas chromatography-mass spectrometric data were collected on an Agilent 6890 N Gas Chromatograph interfaced with quadrupole mass analyzer (Quattro Micro GC, Waters Corporation, Milford MA). A 5% phenyl, methyl silicone stationary phase (HP-5 MS), 15 metre column with a 0.25′ ID was used. The carrier gas was helium and constant flow mode was used to maintain 1.5 ml min^{-1}. Injections of 1.0 µl were made into the injector port heated to 240 °C and a split ratio of 20 : 1 was used. The GC thermal gradient was an initial 30 °C with a 1 min hold after which the temperature was increased 15 °C min^{-1} to a final temperature of 300 °C and held for 2 min. Ionization was by electron impact at 70 eV and the mass analyzer scanned from 45 to 600 u in 0.5 s. The analyzers were tuned to 0.6 u FWHH and data collected in centroid mode.

Ligand synthesis

1,4-Bis(2-pyridylmethyl)piperazine ($L^6py_2{}^H$), 1,4-bis(2-pyridylmethyl)-1,4-diazepane ($L^7py_2{}^H$) and 1,4-bis(6-methyl-2-pyridylmethyl)-1,4-diazepane ($L^7py_2{}^{6\text{-}Me}$) were prepared as previously described.[30,31] The ligands 1,4-bis(4-methyl-2-pyridylmethyl)-1,4-diazepane ($L^7py_2{}^{4\text{-}Me}$) and 1,4-bis(2-quinolinylmethyl)-1,4-diazepane (L^7q_2) were respectively prepared by reacting homopiperazine with 4-methylpicolinaldehyde or quinoline-2-carboxaldehyde (67% and 63% yield), using similar procedures. ^{1}H NMR data (400 MHz) for $L^7py_2{}^{4\text{-}Me}$, and L^7q_2 are as follows: $L^7py_2{}^{4\text{-}Me}$ ($CDCl_3$; δ) 8.36 (d, 2H J_{HH} = 4.04), 7.28 (s, 2H), 6.96 (br d, 2H, J_{HH} = 3.88), 3.77 (s, 4H), 2.81 (t, 4H, J_{HH} = 4.84), 2.77 (s, 4H), 2.34 (s, 6H) 1.85 (p, 2H, J_{HH} = 4.56): L^7q_2 ($CDCl_3$; δ) 8.12–8.05 (m, 4H), 7.79–7.65 (m, 6H), 7.51–7.49 (m, 2H), 3.99 (s, 4H), 2.85 (t, 4H, J_{HH} = 6.00), 2.83 (s, 4H), 1.86 (p, 2H, J_{HH} = 6.44). 1,5-Bis(2-pyridylmethyl)-1,5-diazacyclooctane ($L^8py_2{}^H$) was prepared by a previously reported substitution reaction, where 1,5-diazacyclooctane dihydrobromide is reacted with 2-picolyl chloride hydrochloride.[30] 1,5-Bis((6-methyl-2-pyridyl)methyl)-1,5-diazacyclooctane ($L^8py_2{}^{6\text{-}Me}$) was prepared by the same procedure using 2-(bromomethyl)-6-methylpyridine (42% yield). ^{1}H NMR data (400 MHz) $L^8py_2{}^{6\text{-}Me}$ are as follows: ($CDCl_3$; δ) 7.55–7.51 (m,

2H), 7.34 (d, 2H, J_{HH} = 7.68), 7.00 (d, 2H, J_{HH} = 7.48), 3.79 (s, 4H), 2.79 (t, 8H, J_{HH} = 5.88), 2.51 (s, 6H), 1.67 (p, 4H, J_{HH} = 5.84).

Preparation of manganese(II) complexes

Caution! While no problems were encountered during this work, care should always be taken when handling perchlorate salts of metal complexes because of the possibility of explosion.

The $[Mn^{II}(L^7py_2{}^R)](ClO_4)_2$ (R = H, 6-Me, and 6-MeO) complexes were prepared by a previously reported metalation reaction.[20] The other metal complexes were synthesized with excellent yields (>85%) by reacting $L^6py_2{}^H$, $L^7py_2{}^{4\text{-Me}}$, L^7q_2, and $L^8py_2{}^R$ (R = H and 6-Me) ligands with $Mn(ClO_4)_2$ or $Mn(OTf)_2$ in MeCN solution in a 1 : 1 molar ratio. $Mn(OTf)_2$ was prepared by a previously reported procedure by reacting equimolar amounts of $(CH_3)_3Si(OTf)$ and anhydrous $MnCl_2$.[15] Details of a representative preparation for a metal complex are as followed. To a stirred solution of 277 mg (0.785 mmol) of $Mn(OTf)_2$ in 10 mL of MeCN was added L^7q_2 (300 mg, 0.785 mmol) in 10 mL of MeCN. The yellow solution was stirred overnight and evaporated under reduced pressure. The solid thus obtained was dried in vacuo. Recrystallization of the crude solid from MeCN–diethyl ether afforded nearly colorless crystals of $[Mn(L^7q_2)](OTf)_2$. (505 mg, 87%) [Found for $[Mn(L^7q_2)](OTf)_2$: $C_{27}H_{26}F_6MnN_4O_6S_2$: C, 43.6; H, 3.5; N, 7.4%; M^+ ($\{[Mn(L^7q_2)](OTf)\}^+$) 586.1. $C_{27}H_{26}F_6MnN_4O_6S_2$ requires: C, 44.1; H, 3.6; N, 7.6%; M^+, 586.1], [Found for $[Mn(L^6py_2{}^H)](OTf)_2$: $C_{18}H_{20}F_6MnN_4O_6S_2$: C, 34.4; H, 3.2; N, 8.8%; M^+ ($\{[Mn(L^6py_2{}^H)](OTf)\}^+$) 472.1. $C_{18}H_{20}F_6MnN_4O_6S_2$ requires: C, 34.8; H, 3.2; N, 9.0%; M^+, 472.1], [Found for $[Mn(L^7py_2{}^{4\text{-Me}})](OTf)_2$: $C_{21}H_{26}F_6MnN_4O_6S_2$: C, 38.0; H, 3.8; N, 8.4%; M^+ ($\{[Mn(L^7py_2{}^{4\text{-Me}})](OTf)\}^+$) 514.1. $C_{18}H_{20}F_6MnN_4O_6S_2$ requires: C, 38.0; H, 4.0; N, 8.4%; M^+, 514.1], [Found for $[Mn(L^8py_2{}^H)](OTf)_2$: $C_{20}H_{24}F_6MnN_4O_6S_2$: C, 37.1; H, 3.5; N, 8.5%; M^+ ($\{[Mn(L^8py_2{}^H)](OTf)\}^+$) 500.1. $C_{20}H_{24}F_6MnN_4O_6S_2$ requires: C, 37.0; H, 3.7; N, 8.6%; M^+, 500.1], and [Found for $[Mn(L^8py_2{}^{6\text{-Me}})](OTf)_2$: $C_{22}H_{28}F_6MnN_4O_6S_2$: C, 39.0; H, 4.0; N, 8.2%; M^+ ($\{[Mn(L^7py_2{}^{4\text{-Me}})](OTf)\}^+$) 514.1. $C_{22}H_{28}F_6MnN_4O_6S_2$ requires: C, 39.0; H, 4.2; N, 8.3%; M^+, 514.1].

X-Ray crystallography

Single crystals of $[Mn(L^6py_2{}^H)(CH_3CN)_3](ClO_4)_2$, $[Mn(L^7py_2{}^{4\text{-Me}})(OTf)_2]$, $[Mn(L^7q_2{}^H)(ClO_4)_2]$, $[Mn(L^8py_2{}^H)(ClO_4)_2]$, and $[Mn(L^8py_2{}^{6\text{-Me}})(OTf)_2]$ were grown by vapor diffusion of diethyl ether into an MeCN solution of the complex at room temperature. Data collection and refinement parameters are summarized in the ESI.†

In situ preparation of peroxomanganese(III) complexes

The green peroxomanganese(III) intermediates were formed by treating a 2.5 mM MeCN solution of metal complex with 5 equivalents H_2O_2 and 0.5 equivalents triethylamine at –40 °C. The formation of the peroxomanganese(III) complexes was evident from the appearance of characteristic bands in the electronic absorption spectra and ESI-mass spectrometry. [Found M^+ $\{[Mn^{III}(O_2)(L^7q_2)]\}^+$: 469.1. $\{[Mn^{III}(O_2)(L^7q_2)]\}^+$ requires: M^+, 469.1], [Found M^+ $\{[Mn^{III}(O_2)(L^7py_2{}^{4\text{-Me}})]\}^+$: 397.1. $\{[Mn^{III}(O_2)(L^7py_2{}^{4\text{-Me}})]\}^+$ requires: M^+, 397.1], and [Found M^+ $\{[Mn^{III}(O_2)(L^8py_2{}^H)]\}^+$: 383.1. $\{[Mn^{III}(O_2)(L^8py_2{}^H)]\}^+$ requires: M^+, 383.1]

Kinetic and reactivity studies

Kinetic analyses of aldehyde deformylation were carried out by adding excess CCA to 2.5 mM acetonitrile solutions of $[Mn^{III}(O_2)(L^7py_2{}^R)]^+$ or $[Mn^{III}(O_2)(L^8py_2{}^H)]^+$ and monitoring the time-dependent decay of the characteristic bands of the Mn^{III}–O_2 intermediates at –40 °C in MeCN. Kinetic measurements were made under pseudo-first-order conditions, which permitted the determination of k_{obs} values by fitting the decrease of absorption bands at ~23 000 cm^{-1}. Corresponding second-order-rate constants were obtained using k_{obs} values collected over a range of CCA concentrations. A 2.5 mM solution of $[Mn^{III}(O_2)(L^7py_2{}^H)](OClO_3)$ and $[Mn^{III}(O_2)(L^7py_2{}^H)](OTf)$ was reacted with 120 equivalents of CCA to compare if counter anion had any role on the pseudo first-order rate. The identity of the counteranion had no effect on the rate (k_{obs}).

Product analysis was determined using GC-MS and percent yield was determined by comparing the ratio of the product to an internal standard and comparing the ratio to a standard curve for the product. A detailed procedure is a follows: an approximately 10 mM solution of the peroxometal complex (formed by treating 10 mM solution of the manganese(II) precursor with 5 equivalents H_2O_2 in the presence of 0.5 equivalents Et_3N) was reacted with 120 equivalents of CCA at –40 °C. When the reaction was completed, it was allowed to warm to room temperature, and 1,2-dichlorobenzene was added as an internal standard. A blank run, which lacked only the manganese(II) complex, showed formation of neither cyclohexanone nor cyclohexene.

The Hammett study was preformed by reacting a 2.5 mM acetonitrile solution of $[Mn^{III}(O_2)(L^7py_2{}^H)]^+$ with benzaldehyde, 4-methylbenzaldehyde, 4-methoxybenzaldehyde, or 4-chlorobenzaldehyde under pseudo-first-order conditions, which permitted the determination of k_{obs} values by fitting the decrease absorption band at ~23 000 cm^{-1}.

Density functional theory calculations

The *ORCA* 2.7 software package was used for all DFT computations.[32] Initial models of $[Mn^{III}(O_2)(L^7py_2{}^R)]^+$ (R = H, 4-Me, and 6-Me) were built using the X-ray coordinates of the corresponding manganese(II) complexes, then adding side-on peroxo ligands, and then rotated the pyridines from a canted position to a planar position. Geometry optimizations for each model of the metal complexes were converged to the $S = 2$ spin system. These calculations employed the Becke-Perdew (BP86) functional[33,34] and the SVP (Ahlrichs split valence polarized)[35,36] basis with the SV/C auxiliary basis for all atoms except for manganese, nitrogen, and oxygen, where the larger TZVP (Ahlrichs triple-ζ valence polarized)[20] basis in conjunction with the TZV/J auxiliary basis were used. The resolution of identity (RI) approximation, developed by Neese,[37] was used for all calculations. Solvation effects associated with acetonitrile (dielectric constant ε = 36.6) were incorporated using COSMO, as implemented in *ORCA*.[38]

Acknowledgements

The authors acknowledge the University of Kansas for start-up support, the KU New Faculty General Research Fund and the American Chemical Society Petroleum Research Fund (50287-DNI3) for support. The authors thank the National Science Foundation (Grant CHE-00079282) and KU for funds to purchase the X-ray instrument and computers.

References

1 M. Momenteau and C. A. Reed, *Chem. Rev.*, 1994, **94**, 659–698.
2 J. J. Woodward, M. M. Chang, N. I. Martin and M. A. Marletta, *J. Am. Chem. Soc.*, 2009, **131**, 297–305.
3 A. J. Wu, J. E. Penner-Hahn and V. L. Pecoraro, *Chem. Rev.*, 2004, **104**, 903–938.
4 A.-F. Miller, *Curr. Opin. Chem. Biol.*, 2004, **8**, 162–168.
5 L. E. Grove and T. C. Brunold, *Comments Inorg. Chem.*, 2008, **29**, 134–168.
6 J. A. Cotruvo and J. Stubbe, *Biochemistry*, 2010, **49**, 1297–1309.
7 A. Willing, H. Follmann and G. Auling, *Eur. J. Biochem.*, 1988, **170**, 603.
8 C. Bull, E. C. Niederhoffer, T. Yoshida and J. A. Fee, *J. Am. Chem. Soc.*, 1991, **113**, 4069–4076.
9 A. S. Hearn, C. K. Tu, H. S. Nick and D. N. Silverman, *J. Biol. Chem.*, 1999, **274**, 24457–24460.
10 J. Hayden and M. Hendrich, *JBIC, J. Biol. Inorg. Chem.*, 2010, **15**, 729–736.
11 N. Cox, H. Ogata, P. Stolle, E. Reijerse, G. Auling and W. Lubitz, *J. Am. Chem. Soc.*, 2010, **132**, 11197–11213.
12 T. A. Jackson, A. Karapetian, A.-F. Miller and T. C. Brunold, *Biochemistry*, 2005, **44**, 1504–1520.
13 R. B. VanAtta, C. E. Strouse, L. K. Hanson and J. S. Valentine, *J. Am. Chem. Soc.*, 1987, **109**, 1425–1434.
14 N. Kitajima, H. Komatsuzaki, S. Hikichi, M. Osawa and Y. Moro-oka, *J. Am. Chem. Soc.*, 1994, **116**, 11596–11597.
15 M. S. Seo, J. Y. Kim, J. Annaraj, Y. Kim, Y.-M. Lee, S.-J. Kim, J. Kim and W. Nam, *Angew. Chem., Int. Ed.*, 2007, **46**, 377–380.
16 J. Annaraj, J. Cho, Y.-M. Lee, S. Y. Kim, R. Latifi, S. P. de Visser and W. Nam, *Angew. Chem., Int. Ed.*, 2009, **48**, 4150–4153.
17 R. L. Shook, W. A. Gunderson, J. Greaves, J. W. Ziller, M. P. Hendrich and A. S. Borovik, *J. Am. Chem. Soc.*, 2008, **130**, 8888–8889.
18 S. Groni, G. Blain, R. Guillot, C. Policar and E. Anxolabéhère-Mallart, *Inorg. Chem.*, 2007, **46**, 1951–1953.
19 S. Groni, P. Dorlet, G. Blain, S. Bourcier, R. Guillot and E. Anxolabéhère-Mallart, *Inorg. Chem.*, 2008, **47**, 3166–3172.
20 R. A. Geiger, S. Chattopadhyay, V. W. Day and T. A. Jackson, *J. Am. Chem. Soc.*, 2010, **132**, 2821–2831.
21 U. P. Singh, A. K. Sharma, S. Hikichi, H. Komatsuzaki, Y. Moro-oka and M. Akita, *Inorg. Chim. Acta*, 2006, **359**, 4407–4411.
22 N. Kitajima, H. Fukui and Y. Moro-oka, *J. Am. Chem. Soc.*, 1990, **112**, 6402–6403.
23 J. Annaraj, Y. Suh, M. S. Seo, S. O. Kim and W. Nam, *Chem. Commun.*, 2005, 4529–4531.
24 Y. Goto, S. Wada, I. Morishima and Y. Watanabe, *J. Inorg. Biochem.*, 1998, **69**, 241–247.
25 S. E. Ghachtouli, A. Mohamadou and J.-P. Barbier, *Inorg. Chim. Acta*, 2005, **358**, 3873–3880.
26 S. I. M. Paris, Ü. A. Laskay, S. Liang, O. Pavlyuk, S. Tschirschwitz, P. Lönnecke, M. C. McMills, G. P. Jackson, J. L. Petersen, E. Hey-Hawkins and M. P. Jensen, *Inorg. Chim. Acta*, 2010, **363**, 3390–3398.
27 S. Wang and T. D. Westmoreland, *Inorg. Chem.*, 2009, **48**, 719–727.
28 J. C. Dabrowiak, L. A. Nafie, P. S. Bryan and A. T. Torkelson, *Inorg. Chem.*, 1977, **16**, 540–544.
29 W. L. F. Armarego, and D. D. Perrin, *Purification of Laboratory Chemicals*, Butterworth-Heinemann, Oxford, U.K., 1997.
30 J. A. Halfen, J. M. Uhan, D. C. Fox, M. P. Mehn and L. Que, Jr., *Inorg. Chem.*, 2000, **39**, 4913–4920.
31 R. Mayilmurugan, H. Stoeckli-Evans and M. Palaniandavar, *Inorg. Chem.*, 2008, **47**, 6645–6658.
32 F. Neese, *ORCA - an ab initio, Density Functional and Semiempirical Program Package, Version 2.7*, University of Bonn, 2009.
33 A. D. Becke, *J. Chem. Phys.*, 1986, **84**, 4524–4529.
34 J. P. Perdew, *Phys. Rev. B*, 1986, **33**, 8822–8824.
35 A. Schäfer, H. Horn and R. Ahlrichs, *J. Chem. Phys.*, 1992, **97**, 2571–2577.
36 G. Schäfer, C. Huber and R. Ahlrichs, *J. Chem. Phys.*, 1994, **100**, 5829–5835.
37 F. Neese, *J. Comput. Chem.*, 2003, **24**, 1740–1747.
38 S. Sinnecker, A. Rajendran, A. Klamt, M. Diedenhofen and F. Neese, *J. Phys. Chem. A*, 2006, **110**, 2235–2245.